Int. J. Heat Mass Transfer. Vol. 15, pp. 831–852. Pergamon Press 1972. Printed in Great Britain

INVESTIGATION OF LIQUID DROP EVAPORATION IN A HIGH TEMPERATURE AND HIGH PRESSURE ENVIRONMENT

R. L. MATLOSZ
Captain, U.S. Marine Corps

S. LEIPZIGER
Institute of Gas Technology, Chicago, Illinois 60616, U.S.A.

and

T. P. TORDA
IIT Research Institute, Illinois Institute of Technology, Chicago, Illinois 60616, U.S.A.

(*Received* 25 *May* 1971 *and in revised form* 19 *August* 1971)

Abstract—The phenomena of droplet evaporation in a stagnant environment at high temperature and high pressure has been investigated experimentally and analytically. Experimental droplet temperature–time and radius–time histories have been obtained for n-hexane droplets evaporating in a nitrogen and also an argon gas environment. The ambient gas temperature for all experimental droplet evaporation runs was 548°K; the environment gas pressure was 6·8, 20·4, 40·8, 81·6 and 102 atm; the initial droplet diameter was grouped into two ranges, i.e. the 720–910 μ dia. range and the 1420–1780 μ dia. range.

A theory for droplet evaporation has been developed which (a) accounts for the transient character of the phenomena, (b) includes the effect of the motion of the droplet boundary thus relaxing the quasi-stationary approximation that has been made in previous droplet evaporation theories, and which (c) accounts for the effects of the non-ideal gas behavior for the calculation of the vapor–liquid equilibrium mole fraction boundary condition and for the effects of the non-ideality of the enthalpy of vaporization. The effects of the non-ideal behavior of the gas phase were found to be important for the theoretical predictions of the droplet temperature–time and radius–time histories of evaporating droplets especially at the higher pressures. The results of the comparison of the theoretical prediction for the droplet temperature–time and radius–time histories to the experimental measurements indicated that, at the higher pressures, molecular mass transport may not be the controlling mechanism for the evaporation process. While at the low 6·8 atm pressure the effective mass diffusion coefficient was in good agreement with the formula calculated molecular mass diffusion coefficient, the effective mass diffusion coefficient was more than six times greater than the formula calculated molecular mass diffusion coefficient at 102 atm.

NOMENCLATURE

C_A, partial molar density [gmole/cm^3];

C_g, molar density of the gas phase mixture [gmole/cm^3];

C_L, molar density of the liquid [gmole/cm^3];

C^*, Dimensionless concentration defined by

$$C^* = \frac{C_A}{\bar{C}_g(r \to \infty)};$$

$\bar{C}_g$, film molar density of the gas phase mixture defined by

$$\bar{C}_g = [C_g(r \to \infty) + C_g(R, t)]/2$$

[gmole/cm^3];

$\bar{C}_{P_m}$, film mixture molar heat capacity defined by

$$\bar{C}_{P_m} = X_{A_f} C_{P_A} + (1 - X_{A_f}) C_{P_B}$$

[cal/gmole °K];

C_{P_A}, C_{P_B}, molar heat capacities of components A and B respectively [cal/gmole °K];

$\bar{C}_{SH}$, molar heat capacity of the liquid [cal/gmole °K];

D, diffusion coefficient [cm^2/s];

D_{eff}, effective diffusion coefficient [cm^2/s];

D_M, molecular diffusion coefficient [cm^2/s];

$\bar{e}_L$, energy/mole of the liquid [cal/gmole];

$\bar{e}_S$, energy/mole of component A vapor at the temperature of the liquid droplet [cal/gmole];

f_A, fugacity of component A [atm];

$\bar{H}_L$, enthalpy of the liquid [cal/gmole];

$\tilde{H}_A$, partial molar enthalpy of component A [cal/gmole];

K_V, thermal conductivity of the gas phase mixture [cal/cms °K];

N_{Le}, Lewis number;

P, pressure [atm];

P_V, vapour pressure of the pure component A [atm];

P_T, ambient (total) pressure [atm];

r, radial coordinate [cm];

r^*, dimensionless radius defined by

$$r^+ = \frac{r}{R_0};$$

R, radius of droplet [cm, μ] or gas constant [cal/gmole °K];

R_0, initial radius of droplet [cm, μ];

R^*, dimensionless droplet radius defined by

$$R^* = \frac{R}{R_0};$$

$\dot{R}$, droplet surface velocity [cm/s];

T, temperature [°K];

T^*, dimensionless temperature defined by

$$T^* = \frac{T_\infty - T}{T_\infty};$$

T_∞, ambient temperature [°K];

T_L, temperature of the liquid droplet [°K];

$T_L(\tau = 0)$, initial temperature of the liquid droplet [°K];

$\dot{T}$, rate of change of the droplet temperature;

$\bar{T}_L$, mean temperature of the liquid droplet defined by

$$\bar{T}_L = \frac{1}{t_V}\int_0^{t_V} T_L(\tau)\,\mathrm{d}\tau$$

[°K];

T_{gf}, film temperature of the gas phase defined by $T_{gf} = (\bar{T}_L + T_\infty)/2$ [°K];

t, time [s];

t_v, droplet evaporation time [s];

t^*, dimensionless time defined by

$$t^* = \frac{Dt}{R_0^2};$$

u, molar averaged radial velocity [cm/s];

$\bar{V}_L$, molar volume of the liquid [cm^3/mole];

$\tilde{V}_i$, partial molar volume of component i [cm^3/gmole];

X_A, mole fraction of component A defined by $X_A = C_A(R, t)/C_g(R, t)$;

Z, compressibility factor

$$Z = \frac{PV}{RT};$$

α, ratio of the liquid molar density to gas phase molar density evaluated at the liquid–gas interface

$$\alpha = C_L/C_g(R, t);$$

α_∞, ratio of the liquid molar density to gas phase molar density evaluate at infinity

$$\alpha_\infty = C_L/C_g(r \to \infty);$$

α_K, thermal diffusion coefficient [cm^2/s];

β, ratio of the molar heat capacity in the gas mixture to the molar heat capacity of the liquid

$$\beta = \bar{C}_{p_m}/\bar{C}_{SH};$$

γ, dimensionless quantity defined by

$$\gamma = \lambda/\bar{C}_{SH}T_\infty;$$

δ, dimensionless quantity defined by

$$\delta = 1 - \frac{\eta\gamma}{\varphi};$$

η, derivative with respect to dimensionless temperature of the natural logarithm of the molar density

$$\eta = \frac{\mathrm{d}\ln(C_L)}{\mathrm{d}T};$$

λ, heat of vaporization [cal/gmole];
μ_A, chemical potential [cal/gmole];
ν_L, moles of liquid [gmoles];
τ, dimensionless time variable;
φ, dimensionless quantity defined by

$$\varphi = 1 + \eta\gamma;$$

φ_A^V, fugacity coefficient of component A in the gas phase;
ψ, dimensionless space variable.

INTRODUCTION

THE PHENOMENA associated with the evaporation of a single droplet and the methods of predicting its evaporation rate are important in the analysis of engineering operation involving the processes of spray cooling, drying, absorption, desorption, humidification and combustion. Extensive literature, concerning both experimental and theoretical research, is available on the subject of single droplet evaporation in a stagnant environment or under forced convective conditions at atmospheric or near atmospheric pressures.

In many applications, for example, internal combustion engine operation (both gasoline and diesel engines), droplet evaporation at elevated pressures and temperatures is important. Knowledge of liquid droplet evaporation rates at elevated pressures and temperatures is particularly important for the design of high-output combustors for aircraft jet engines. In jet engines, as discussed by Ingebo, [1] the fuel is frequently injected in liquid droplet form at a point upstream of the combustion zone. The concentration of the fuel vapor in the fuel–air stream entering this zone is determined by the rate of evaporation of the droplets. In Ingebo's experimental investigation, the evaporation rates of pure liquid drops were determined under conditions similar to those encountered in aircraft combustion systems. A wetted cork sphere, simulating a drop of liquid, was placed in an air stream of constant mass-flow rate and of varying temperature. Liquid was injected into the sphere at a rate equal to the evaporation rate, and the loss of liquid from the sphere's surface was determined. The resulting data on evaporation rates were found to correlate with a semiempirical theory of heat and mass transfer. Ingebo's work triggered a series of experimental and theoretical investigations of single droplet evaporation aimed at their behavior in high performance combustors. Ingebo followed up his first study by considering the pressure effects on droplet evaporation (air stream static pressure range of 450–1500 mm of Hg). [2] His experimental procedure was similar to that used in his first investigation except that the gas environment was pressurized. Ranz and Marshall, [3] although interested in spray drying processes, used an experimental method similar to Ingebo's and introduced the widely accepted concept of heat and mass transfer analogies for spheres in natural and forced convection environment. In all the experimental investigations mentioned, heat and mass transfer coefficients for spheres were developed from steady state

semiempirical correlations and the pressure effects on these transfer coefficients were obtained. In these experimental studies, no consideration of the transient behavior of an evaporating droplet is given. However, El Wakil, Uyehara and Myers in a series of three monographs [4–6] used the Ranz and Marshall correlations to develop a quasi-steady, transient phenomenological model for single droplet evaporation in stagnant and forced convective environments. Their work also included experimental investigations which agreed with the predictions of the semiempirical theory. Although this study was the first comprehensive investigation of droplet evaporation in stagnant and flowing environments, the work was limited to droplet evaporation at atmospheric or near atmospheric pressures.

With the advent of the liquid propellant rocket motors, the knowledge of liquid droplet evaporation rates became important in still another application. Analytical models have been formulated for the design of liquid propellant rocket motors correlating the design parameters such as chamber pressure and temperatures, gas velocities and chamber geometries [7–9]. In some of these analyses, propellant evaporation is assumed to be the rate controlling process. It is for this reason that the prediction of evaporation rates at high chamber pressures and temperatures is important. The justification of the assumption that the evaporation process is the rate controlling step is based on the findings of Heidmann, Priem and Humphrey, [10], Bittker, [11], and Bittker and Brokaw [12] concerning the time and distance required for atomization, mixing and chemical reactions. However, the results based on the evaporation rate controlled model at high chamber pressures is questionable, since there is a lack of understanding concerning the evaporation phenomena in supercritical gas environments (high chamber pressures and temperatures). As used here, the term supercritical means a gaseous environment whose temperature and pressure are greater than the thermodynamically defined critical temperature and critical pressure of the pure component. In the loose sense (which is widely accepted) the supercritical environment would be a gaseous environment (any gas) that has a temperature and pressure greater than the critical temperature and pressure of the liquid.

Torda [13, 14] indicated that liquid propellant droplets evaporating in a supercritical environment may remain in a transient heating state during the phase change contrary to the assumed "normal" process. The "normal" process is defined as droplet evaporation at a constant temperature where all the energy arriving at the droplet surface is used to vaporize the liquid and no energy is available for changing the temperature of the droplet. Such a process has been used in all design and combustion instability studies to date. Torda concluded that a thorough investigation of the mechanism of droplet evaporation at elevated pressures and temperatures is a necessary requirement for a more valid model for rocket design and instability studies. Hypotheses about the phenomena of droplet evaporation under supercritical conditions have been either: (1) that the droplets are heated to an equilibrium wet-bulb temperature somewhat below the critical temperature, or (2) that the droplets undergo transient heating through the critical temperature [15]. Wieber [16] has shown that it is posssible to predict analytically which of these two characteristic modes of behavior will take place under particular conditions depending upon how much of a droplet's mass is involved and how long the liquid-to-vapor transformation processes take. Combs [15] concluded from Wieber's analysis that if a droplet heats through its critical temperature it will no longer exhibit liquid properties but exist as dense pockets of supercritical "fluid". The subsequent combustion rate would be controlled not by propellant evaporation but by the turbulent diffusion and mixing of the propellant vapors [17].

Wieber's analysis of the calculated temperature histories of vaporizing droplets to the

critical point has been widely accepted and used in the existing analytical modeling of liquid rocket engine combustion instability studies. The foremost objection in the analysis is that the theory for droplet evaporation has been developed at temperatures and pressures appreciably below the critical point of the fluid, whereas, a major fraction of the droplet's lifetime may be spent either in transient heating to its critical temperature while evaporating, or at some wet-bulb temperature below its critical temperature. Another objection in the analysis is the quasi-steady assumption of droplet evaporation, but Wieber indicated that at the very worst, the analysis defines the upper limit of application of the theory, which is, the droplet heating to the critical temperature. Other investigators [18, 19] disagree with this conclusion indicating that, for environmental gas pressures greater than one-tenth the critical pressure of the vaporizing liquid, the quasi-steady vaporization theory is not valid.

It became apparent that experimental evaporation histories in supercritical environments were necessary either to verify existing theories or to formulate an improved theory. These experimental evaporation histories had to include the mass, radius and temperature–time variations for single droplets in varying high temperature and high pressure environments. The more fundamental problem of droplet evaporation in a stagnant environment was thought to be a first step in the understanding of the supercritical evaporation phenomena encountered in rocket engines. Although the problem of droplet evaporation in a stagnant environment departs grossly from the real situation encountered in rocket combustors, the evaporation mechanism of a single stationary droplet, nevertheless, serves as a first indicator, or perhaps, as a reference in the behaviour of propellants. Preliminary results from this research program have been published [20–22]. The results presented in this paper are extensions and improvements on this previous work.

FORMULATION OF THE MATHEMATICAL MODEL

The mathematical analysis presented here combines and extends some of the ideas found in the literature. This analysis extends the mathematical model formulated by Williams [23], capitalizes on the sophisticated mathematical methods for solving the transient diffusion equation subject to a moving boundary developed by Duda and Vrentas [24], and includes the important non-ideal gas effects for droplet evaporation at high ambient pressure and temperature that were investigated by Manrique and Borman [25].

Consider a single-component liquid droplet evaporating in an inert gaseous environment infinite in extent. The evaporation process is controlled by the transport of energy and matter in the gas phase. The liquid droplet is considered a perfect, isolated, fixed sphere and the transport processes occurring in the infinite gaseous atmosphere are dependent only on the radial distance from the center of the sphere and time. Uniform temperature inside the liquid droplet is assumed and the solubility of the gas phase in the liquid droplet is neglected. Constant mass diffusion coefficient and constant thermal conductivity of the gas mixture are also assumed. To simplify the calculation of the concentration and temperature profiles in the boundary layer, the mixture molar density and the mixture heat capacity are assumed constant and are assigned an arithmetic averaged film value. For boundary condition calculations, however, the value of the mixture molar density is determined by the temperature, pressure, and concentration of the binary mixture at the liquid–gas boundary.

Under these conditions, the equation of continuity for component A (the evaporating component) in the gas phase is

$$\frac{\partial C_A}{\partial t} = \frac{D}{r^2}\frac{\partial}{\partial r}\left[r^2\frac{\partial C_A}{\partial r}\right] - \frac{R^2}{r^2}u(R,t)\frac{\partial C_A}{\partial r} \qquad (1)$$

where R is the droplet radius and $u(R, t)$ is the radial velocity at the liquid–gas interface.

Similarly, the equation for conservation of energy may be written

$$\frac{\partial T}{\partial t} = \frac{\alpha_D}{r^2}\frac{\partial}{\partial r}\left[r^2\frac{\partial T}{\partial r}\right] - \frac{R^2}{r^2}u(R,t)\frac{\partial T}{\partial r} \tag{2}$$

where

$$\alpha_D = K_v/\bar{C}_g\bar{C}_{p_m}$$

is the thermal diffusivity.

A material balance written for the droplet gives

$$-\frac{dv_L}{dt} = 4\pi R^2 C_g(R,t)[u(R,t) - \dot{R}) \tag{3}$$

where v_L is the number of moles of liquid. Expressing the number of moles of liquid in terms of the volume of a sphere and the liquid molar density and taking into account the variation of the liquid molar density with temperature, one obtains

$$-\frac{dv_L}{dt} = -\frac{d}{dt}\left[\frac{4}{3}\pi R^3 C_L\right] = -4\pi R^2\dot{R}C_L - \frac{4}{3}\pi R^3\frac{dC_L}{dT}\frac{dT_L}{dt}. \tag{4}$$

Combining equations (3) and (4) and solving for the radial velocity at the droplet boundary yields

$$u(R,t) = \dot{R}[1-\alpha] - \frac{R\alpha}{3}\frac{d\ln(C_L)}{dT}\frac{dT_L}{dT} \tag{5}$$

where

$$\alpha = C_L/C_g(R,t). \tag{6}$$

Substituting equation (5) into equations (1) and (2) gives for the equation of continuity for component A

$$\frac{\partial C_A}{\partial t} = \frac{D}{r^2}\frac{\partial}{\partial r}\left[r^2\frac{\partial C_A}{\partial r}\right] - \frac{R^2}{r^2} \times\left[\dot{R}(1-\alpha) - \frac{R\alpha}{3}\frac{d\ln(C_L)}{dT}\frac{dT_L}{dt}\right]\frac{\partial C_A}{\partial r} \tag{7}$$

and for the equation for conservation of energy

$$\frac{\partial T}{\partial t} = \frac{\alpha_D}{r^2}\frac{\partial}{\partial r}\left[r^2\frac{\partial T}{\partial r}\right] - \frac{R^2}{r^2} \times\left[\dot{R}(1-\alpha) - \frac{R\alpha}{3}\frac{d\ln(C_L)}{dT}\frac{dT_L}{dt}\right]\frac{\partial T}{\partial r} \tag{8}$$

where the expression for the radial velocity given in equation (5) has been used.

Of the four boundary conditions and one auxiliary (free boundary) condition necessary for the solution of the energy and mass transport equations [equations (7) and (8)], the boundary conditions at the liquid–gas interface are of special significance. Material and energy balance requirements at the droplet interface result in differential equations relating the rate of change of the droplet temperature and droplet radius to the concentration and temperature gradients in the gas phase evaluated at that interface.

A material balance at the droplet surface assuming the inert gas will not diffuse into the liquid allows one to find an expression for the time rate of change of droplet radius. The result is

$$\dot{R} = \frac{D}{C_L(1-X_A)}\left.\frac{\partial C_A}{\partial r}\right|_R - \frac{R}{3}\frac{d\ln(C_L)}{dT}\frac{dT_L}{dt} \tag{9}$$

where

$$X_A = C_A(R,t)/C_g(R,t).$$

An energy balance for the droplet, neglecting work done by the surface forces and viscous dissipation yields

$$\frac{R}{3}C_L\bar{C}_{SH}\frac{dT_L}{dt} = K_v\left.\frac{\partial T}{\partial r}\right|_R + (\bar{e}_S - \bar{e}_L)\left\{-D\left.\frac{\partial C_A}{\partial r}\right|_R + C_A[u(R,t) - \dot{R}]\right\} \tag{10}$$

where $(\bar{e}_S - \bar{e}_L)$ is the energy required for phase change of component A. The usual approximation for the term $(\bar{e}_S - \bar{e}_L)$ is the latent heat of vaporization of the pure component A evaluated at the droplet temperature. Manrique and

Borman [25], however, showed this approximation to be an over-simplification for droplet evaporation at high total pressure where the effect of non-ideal behavior of the gas mixture becomes significant. A discussion on the calculation of the energy requirements for phase change in the presence of an inert gas is presented in the next section.

The remaining boundary condition at the droplet surface is usually expressed by the vapor–liquid equilibrium relationship

$$\left.\frac{C_A}{C_g}\right|_R = X_A(R, t) = H[T(R, t), P_T] \tag{11}$$

where $H[T(R, t), P_T]$ is some function whose value is determined by the droplet temperature, $T(R, t)$ and the total pressure, P_T. The usual approximations for determining the function H are that the gas mixture obeys the equation of state for ideal gases and that the presence of the inert gas does not affect the equilibrium vapor pressure of pure component A at the droplet temperature. With these approximations an expression for the local equilibrium mole fraction is given by

$$X_A(R, t) = P_V[T(R, t)]/P_T \tag{12}$$

where P_V is the vapor pressure of pure component A at the droplet temperature, $T(R, t)$. Manrique and Borman [25] showed that this simplified boundary condition, although perfectly valid at low pressures, fails to be correct at high total pressures. A discussion on the calculation of the vapor–liquid equilibrium function H for real gas mixtures is also presented in the next section.

For completeness the remaining boundary and initial conditions required for the solution of the set of governing partial differential equations [equations (7) and (8)] are stated as follows:

Boundary conditions:

$$r \to \infty \qquad T \to T_\infty \qquad C_A \to 0 \tag{13}$$

Initial conditions:

$$t = 0 \qquad R = R_0 \qquad T = T_\infty \qquad C_A = 0 \qquad R_0 < r < \infty \qquad T(R_0, 0) = T_L(0). \tag{14}$$

The introduction of dimensionless variables

$$C^* = \frac{C_A}{C_g(r \to \infty)}; \quad R^* = \frac{R}{R_0}; \quad T^* = \frac{T_\infty - T}{T_\infty}; \quad t^* = \frac{Dt}{R_0^2}; \quad r^* = \frac{r}{R_0}$$

converts the governing equations to

$$\frac{\partial C^*}{\partial t^*} = \left[\frac{\partial^2 C^*}{\alpha r^{*2}} + \frac{2}{r^*}\frac{\partial C^*}{\partial r^*}\right] - \left(\frac{R^*}{r^*}\right)^2 \times \left[\dot{R}^*(1 - \alpha) - \frac{R^*\alpha}{3}\frac{\mathrm{d}\ln(C_L)}{\mathrm{d}t^*}\frac{\mathrm{d}T_L^*}{\mathrm{d}t^*}\right]\frac{\partial C^*}{\partial r^*} \tag{15}$$

$$\frac{\partial T^*}{\partial t^*} = \frac{1}{N_{Le}}\left[\frac{\partial^2 T^*}{\partial r^{*2}} + \frac{2}{r^*}\frac{\partial T^*}{\partial r^*}\right] - \left(\frac{R^*}{r^*}\right)^2 \times \left[\dot{R}^*(1 - \alpha) - \frac{R^*\alpha}{3}\frac{\mathrm{d}\ln(C_L)}{\mathrm{d}T^*}\frac{\mathrm{d}T_L^*}{\mathrm{d}t^*}\right]\frac{\partial T^*}{\partial r^*} \tag{16}$$

where

$$N_{Le} = \frac{D}{\alpha_D}.$$

At the droplet boundary the results are

$$\dot{R}^* = \frac{1}{\alpha_\infty(1 - X_A)}\frac{\partial C^*}{\partial r^*} - \frac{R^*}{3}\frac{\mathrm{d}\ln(C_L)}{\mathrm{d}T^*}\frac{\mathrm{d}T_L^*}{\mathrm{d}t^*} \tag{17}$$

where

$$\alpha_\infty = C_L/C_g(r \to \infty)$$

$$\frac{R^*}{3}\frac{\mathrm{d}T_L^*}{\mathrm{d}t^*} = \frac{\beta}{2N_{Le}}\left[\frac{1}{\alpha} + \frac{1}{\alpha_\infty}\right]\frac{\partial T^*}{r^*} + \gamma\left[\dot{R}^+ + \frac{R^*}{3}\frac{\mathrm{d}\ln(C_L)}{\mathrm{d}T}\frac{\mathrm{d}T_L^*}{\mathrm{d}t^*}\right] \tag{18}$$

where

$$\lambda = \bar{e}_S - \bar{e}_L$$

$$\beta = \bar{C}_{P_m}/\bar{C}_{SH}$$

$$\gamma = \lambda/\bar{C}_{SH}T_\infty$$

$$C_A = C_A(R,t) \to C^* = X_A(R,t)\left(\frac{\alpha_\infty}{\alpha}\right) \tag{19}$$

and for boundary conditions far removed from the droplet one has

$$\begin{aligned} T = T_\infty &\to T^* = 0 \\ C_A = 0 &\to C^* = 0. \end{aligned} \tag{20}$$

The initial conditions in dimensionless notation become

$$\begin{aligned} t = 0 \qquad & R^* = 1 \\ & T^* = 0 \\ & C^* = 0 \qquad 1 < r^* < \infty \\ & T_L^* = \frac{T_\infty - T_L(0)}{T_\infty}. \end{aligned} \tag{21}$$

Using a suitable transformation, it is convenient to map the infinite gas phase region into a region of finite extent and to immobilize the moving boundary. Considering, then, the transformation

$$\begin{aligned} \psi &= 1 - \exp\left[-(r^* - R^*)\right] \\ \tau &= t^* \end{aligned} \tag{22}$$

it follows that

$$C^*(r^*, t^*) \to C[\psi(r^*, R^*, t^*), \tau(t^*)].$$

The governing partial differential equations become with the superscript (*) dropped

$$\frac{\partial C}{\partial \tau} + F(1-\psi)\frac{\partial C}{\partial \psi} = (1-\psi)^2\frac{\partial^2 C}{\partial \psi^2} + \left[\frac{2}{R - \ln(1-\psi)} - 1\right](1-\psi)\frac{\partial C}{\partial \psi} \tag{23}$$

$$\frac{\partial T}{\partial \tau} + F(1-\psi)\frac{\partial T}{\partial \psi} = \frac{(1-\psi)^2}{N_{Le}}\frac{\partial^2 C}{\partial \psi^2} + \frac{(1-\psi)}{N_{Le}}\left[\frac{2}{R - \ln(1-\psi)} - 1\right]\frac{\partial C}{\partial \psi} \tag{24}$$

where

$$F = \frac{R^2}{\left[R - \ln(1-\psi)\right]} \times \left\{\dot{R}(1-\alpha) - \frac{R\alpha}{3}\eta\dot{T}\right\} - \dot{R} \tag{25}$$

and where

$$\eta = \frac{\mathrm{d}\ln(C_L)}{\mathrm{d}T}. \tag{26}$$

The initial conditions become

$$\begin{aligned} C &= 0 \qquad 0 < \psi \leqslant 1 \\ T &= 0 \qquad 0 < \psi \leqslant 1 \end{aligned} \tag{27}$$

and the boundary conditions far removed from the droplet become

$$\begin{aligned} r \to \infty \qquad \psi \to 1 \qquad & C = 0 \\ & T = 0. \end{aligned} \tag{28}$$

The temperature of the liquid droplet is equal to the temperature of the gas phase evaluated at the droplet boundary and this result can be expressed in terms of the transformed variables as

$$T_L^* = T^*[R^*(t^*), t^*] = T(\psi = 0, \tau).$$

The rate of change of temperature of the liquid droplet, that is, the total derivative of the gas phase temperature evaluated at the droplet boundary, $R(t)$, can be written in terms of transformed variables as

$$\frac{\mathrm{d}T_L^*}{\mathrm{d}t^*} = \left(\frac{\partial T}{\partial \tau}\right)_{\psi=0} = \dot{T}. \tag{29}$$

The boundary conditions at the droplet surface ($\psi = 0$) then reduce to

$$\dot{R} = \frac{1}{\alpha_\infty(1 - X_A)}\frac{\partial C}{\partial \psi} - \frac{R\eta\dot{T}}{3} \tag{30}$$

$$\dot{T} = \frac{3}{2}\frac{\beta}{N_{Le}\varphi R}\left(\frac{1}{\alpha} + \frac{1}{\alpha_\infty}\right)\frac{\partial T}{\partial \psi} - \frac{3}{R}\frac{\gamma}{\varphi}\dot{R} \tag{31}$$

where

$$\varphi = 1 + \eta\gamma.$$

The two unknowns in equations (30) and (31) are the droplet surface velocity, $\dot{R}$, and the rate of change of droplet temperature, $\dot{T}$. Eliminating $\dot{T}$ from equation (30) using equation (31) gives

$$\dot{R} = \frac{1}{\alpha_\infty \delta(1 - X_A)} \frac{\partial C}{\partial \psi} - \frac{\beta\eta}{2N_{Le}\delta\varphi} \times \left[\frac{1}{\alpha} + \frac{1}{\alpha_\infty}\right] \frac{\partial T}{\partial \psi} \quad (32)$$

where

$$\delta = 1 - \frac{\eta\gamma}{\varphi}.$$

The droplet radius, $R(t)$, and the droplet temperature, $T_L(t)$, can be determined, then, by solving the governing equations (23) and (24) subject to the initial conditions given by equation (27) and the boundary conditions given by equations (28), (31) and (32).

NON-IDEAL EFFECTS AND THE EFFECT OF THE INERT GAS

At the droplet surface, thermodynamic equilibrium between the vapor phase mixture and the liquid is assumed to exist and this condition may be represented by the vapor–liquid equilibrium relationship:

$$X_A(R, t) = H[T(R, t)\, P_T] \quad (33)$$

where $T(R, t)$ is the droplet temperature and P_T is the total pressure, and X_A is the mole fraction of n-hexane in the vapor phase at the droplet surface. The function H must be estimated subject to the conditions that the liquid phase is pure component A and that the gas phase (comprising vapor A and inert gas B) is a real, non-ideal gas mixture.

The condition for equilibrium in terms of chemical potentials is

$$\mu_A^L = \mu_A^V. \quad (34)$$

The chemical potential for any component in the system, whether liquid or gas, pure or mixed, ideal or not may be written

$$\mu_i = RT \ln f_i/f_i^0 + \mu_i^0 \quad (35)$$

where f_i is the fugacity and μ_i^0 and f_i^0 are the chemical potential and fugacity respectively at some standard state. Using equations (34) and (35), it may be shown that [28]

$$X_A[T(R, t), P_T] = [P_V \Phi_A^{SL}/P_T \Phi_A^V] \times \exp\left[1/RT \int_{P_V}^{P_T} \bar{V}_L \, dP\right] \quad (36)$$

where P_V is the vapor pressure of pure liquid A at temperature T, P_T is the system pressure, $\bar{V}_L$ is the molar density of the liquid phase, Φ_A^{SL} is the fugacity coefficient of component A at saturated liquid conditions and is given by

$$\Phi_A^{SL} = f_A^{SL}/P_V \quad (37)$$

and Φ_A^V is the vapor phase fugacity coefficient of component A and is given by

$$\Phi_A^V = f_A^V/X_A P_T. \quad (38)$$

Thus at least formally, equation (36) represents an expression for the function H.

All of the quantities on the right hand side of equation (36) except Φ_A^V may be found from thermodynamic and volumetric data for n-hexane. Saturated thermodynamic properties were obtained from Canjar and Manning [26] compressed liquid molar volume data was obtained from Stewart, Sage and Lacey [27].

The fugacity coefficient of component A in the gas mixture can be calculated from the equation

$$\ln \Phi_A^V = (1/RT) \int_0^{P_T} [\tilde{V}_A - RT/P] \, dP. \quad (39)$$

An alternate form of equation (39) with volume replacing pressure as one of the independent variables given by [28–30],

$$RT \ln \Phi_A^V = \int_V^\infty \left[\left(\frac{\partial P}{\partial v_A}\right)_{T, V, v_B} - RT/V\right] dV - RT \ln Z. \quad (40)$$

Since sufficient volumetric data were not available for the gas mixture, it was necessary to use

an equation of state for the gas mixture to calculate the fugacity coefficient. Based on the work of Chuch and Prausnitz [28, 29], the Redlich–Kwong equation of state with a set of mixing rules to calculate vapor phase fugacity coefficients for high pressure systems was chosen.

The procedure for calculating X_A is straightforward. At a given temperature and pressure in which equilibrium is assumed possible, a first estimate of X_A is made by using equation (36) with $\Phi_A^V = 1$. The vapor phase fugacity Φ_A^V assigned unity corresponds to the assumption that the gas mixture behaves ideally. Using the mixing rules the Redlich–Kwong equation of state parameters are calculated for the mixture since X_A and $X_B = 1 - X_A$ are known. The mixture molar volume $\bar{V}$ is calculated by solving the Redlich–Kwong equation of state which is cubic in $\bar{V}$. Then the vapor phase fugacity Φ_A^V is calculated using the integrated form of of equation (40) since the term $(\partial P/\partial v_A)_{T,V,v_B}$ is readily calculated from the Redlich–Kwong equation of state for the mixture [28]. Using equation (36), X_A is recalculated this time using the computed value for Φ_A^V. The entire calculation procedure is iterated until a convergence criteria on X_A is satisfied.

A Fortran computer program was written to calculate the equilibrium mole fraction following the above computational procedure. The simplified ideal gas boundary condition, neglecting the effect of the inert gas, for the equilibrium mole fraction

$$X_A(R, t) = P_V/P_T \qquad (41)$$

was also calculated and compared to the more realistic equilibrium mole fraction, X_A, calculated from analysis. The results of these calculations were compared with the experimental data of Poston and McKetta [31] are also presented and except for the highest isotherm (340°F) there is reasonable agreement between the analysis and experimental data. At the highest isotherm the analysis fails to predict equilibrium mole fraction for pressures greater than 30 atm because the model assumes equilibrium exists for component A only and that the component B is present in the gas phase only, neglecting the solubility of component B in the liquid. A more valid model for the phenomena at this high temperature is one whereby the condition for equilibrium exists for component B as well as for component A. The reason for choosing the former model over the latter one is because the calculation procedure is straightforward and because (from experimental observation) in most cases the liquid temperature lies below this high temperature throughout the droplets' lifetime. Fig. 1 shows the results of these calculations at a temperature of 220°F.

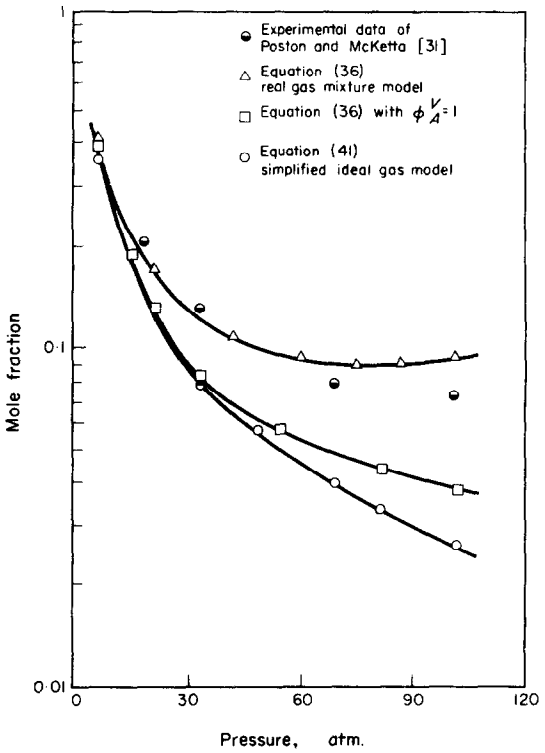

FIG. 1. The variation of the equilibrium mole fraction of n-hexane in the gas phase with total pressure at constant temperature (220°F) for the n-hexane–nitrogen system.

From the results of the above analysis, the non-ideal behavior of the gas mixture must be accounted for (especially at the higher pressures) when estimating the equilibrium mole fraction.

The effect of the non-ideal behavior of the gas mixture on the energy requirements for vaporization is considered next. The deviations between the usually assumed latent heat of vaporization for the pure component and the enthalpy of vaporization which includes the effects of the non-ideal gas mixture are determined using the Redlich–Kwong equation of state [32]. The quantity which is calculated, λ, is given by

$$\lambda = \bar{H}_A[g, T, P_T, X_A] - \bar{H}_L[l, T, P_T]. \quad (42)$$

The results for the calculation of the enthalpy of vaporization, λ, are presented in Fig. 2. The solid line represents the latent heat of vaporization of the pure component A, n-hexane, as a function of the equilibrium temperature [26]. The broken lines represent the heat of vaporization with the non-ideal behavior of the gas mixture included as a function of the equilibrium temperature at various constant total pressures.

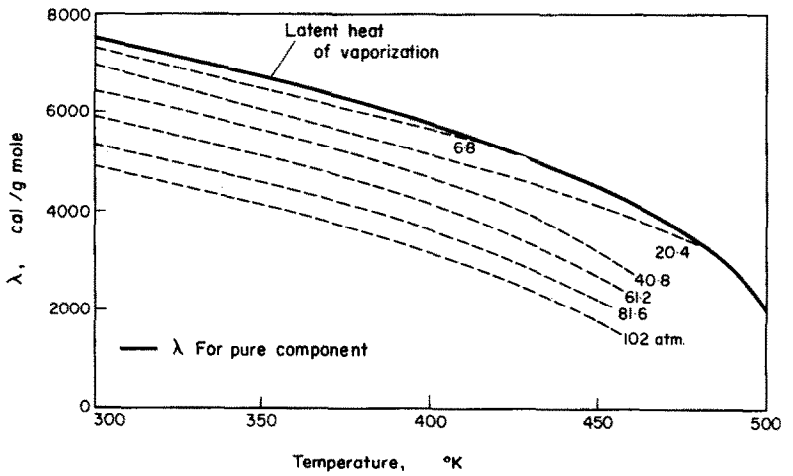

FIG. 2. The energy requirements for phase change.

NUMERICAL SOLUTION

Numerical methods were used to obtain solutions to the governing equations. An implicit finite difference technique employing a slightly modified Crank–Nicholson computational scheme was used to solve the system of partial differential equations.

Theoretical predictions for the temperature-time and radius-time histories were obtained for n-hexane droplets evaporating in nitrogen gas at an ambient temperature of 548°K and for environment pressure of 6·8, 20·4, 40·8, 81·6 and 102 atm. Convergence of the finite difference technique was established by the usual methods of varying the mesh size. The effects of Lewis Number on the droplet temperature–time and radius–time histories for the range of environment pressures were investigated and the results at 6·8 atm and 102 atm are shown in Figs. 3 and 4.

The effects of the types of boundary conditions on the droplet temperature-time and radius–time histories for the range of environment pressures were investigated. The results at 6·8 atm and 102 atm are shown in Figs. 5 and 6. The boundary conditions labeled ideal gas mixture in the figures refer to the simplified vapor–liquid equilibrium condition given by equation (41) and the pure component enthalpy of vaporization for λ. The boundary conditions

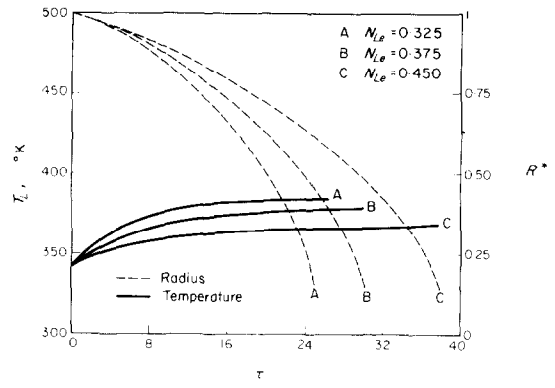

FIG. 3. The effect of Lewis number on the droplet temperature–time and radius–time histories. P = 6·8 atm.

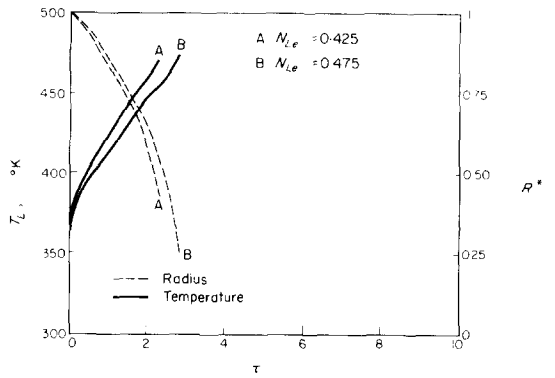

FIG. 4. The effect of Lewis number on the droplet temperature–time and radius–time histories. P = 102 atm.

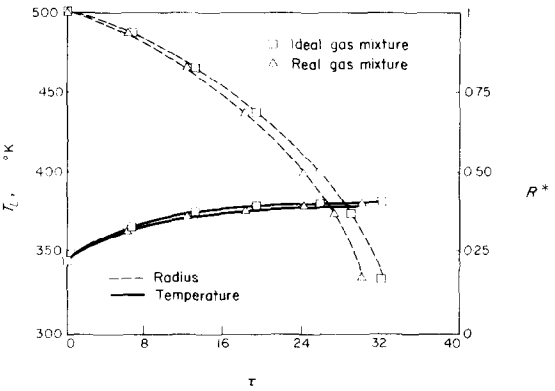

FIG. 5. Comparison of the real with the ideal gas mixture models. P = 6·8 atm.

labeled real gas mixture refer to the vapor–liquid equilibrium condition given by equation (36) and λ given by equation (42). In order to single out the effects of the type of boundary conditions on the evaporation histories, theoretical predictions for the droplet temperature–time and radius–time histories were compared where in one case the vapor–liquid equilibrium given by equation (36) was used and λ was first assigned a value corresponding to the pure component enthalpy of vaporization and then assigned the value calculated from equation (42). In the other case, the pure component enthalpy of vaporization was used for λ and the vapor–liquid equilibrium was determined first from equation (41) and then from equation (36). Although both effects change the results significantly at higher pressures, the influence of the vapor–liquid equilibrium is somewhat greater.

Concentration and temperature profiles in the gas phase were determined and the results for pressures of 20·4 atm and 102 atm are shown in Figs. 7 and 8. The time values given in the figures are the dimensionless times, τ, and the radius values are the dimensionless droplet radius, R/R_0, values at the corresponding dimensionless times. The concentration and temperature values at a given position in the dimensionless ψ space can be related back to the physical space with the aid of the transformation equation

$$r^* = R^* - \ln(1 - \psi).$$

EXPERIMENTAL APPARATUS AND TECHNIQUES

The objectives of the experimental research are to record the temperature and size of a liquid droplet evaporating in a high pressure and high temperature environment. The apparatus for the experimental study consists of a test chamber pressurized with an appropriate gas (nitrogen or argon) and heated to a preselected equilibrium temperature in an electric furnace. The liquid droplet is injected and is suspended from a 0·002 in. chromel–alumel thermocouple to permit measurement of the droplet temperature. The time history of the droplet temperature is recorded using a Type RS2-channel Dynograph

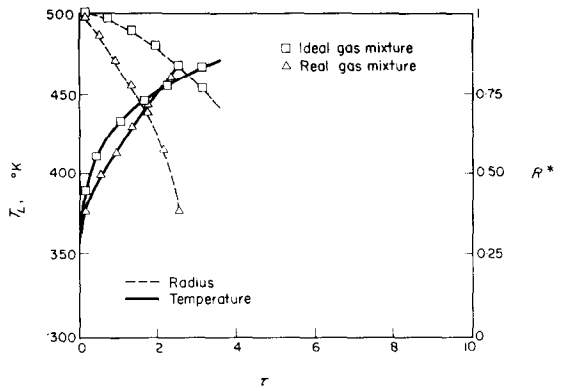

FIG. 6. Comparison of the real with the ideal gas mixture models. $P = 102$ atm.

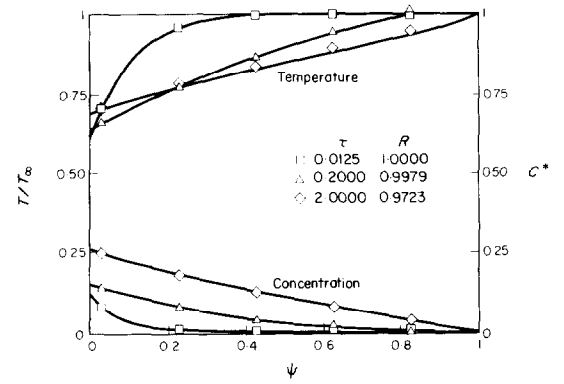

FIG. 7. Concentration and temperature profiles in the gas phase (dimensionless time for evaporation is 14·92). $P = 20{\cdot}4$ atm; $N_{Le} = 0{\cdot}425$.

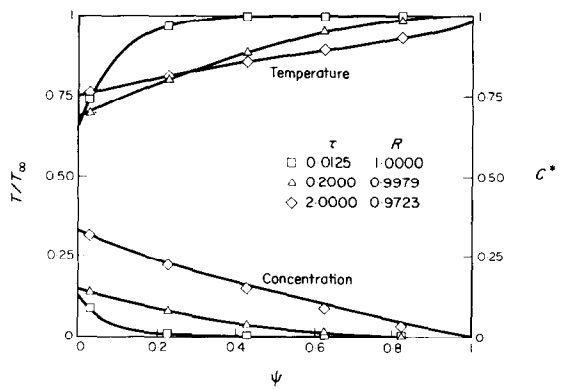

FIG. 8. Concentration and temperature profiles in the gas phase (dimensionless time for evaporation is 2·62). $P = 102$ atm; $N_{Le} = 0{\cdot}425$.

Recorder and the time history of the droplet size is recorded using a Bolex 16 mm movie camera. A schematic drawing of the experimental apparatus is shown in Fig. 9. A detailed explanation of the various equipment that are numbered in the drawing is given following the figure. A brief description of some of the more important parts of the apparatus is presented in the following discussion.

An optical system was built to permit shadowed or silhouetted photography of the droplet image. In the optical setup, a 209·5 mm Bausch and Lomb projection lens is used to project the silhouetted droplet image onto a ground glass screen. The projected silhouetted droplet image is, then, photographed using the Bolex 16 mm movie camera with an 85 mm focal length lens and an attached +3 diopter close-up lens. Using the Bausch and Lomb lens in combination with the Bolex movie camera optics, and overall magnification of the droplet image of approximately 2·0–2·3 was obtained.

An electronic strobe unit was also incorporated into the optical system. The purpose of the strobe unit is to synchronize the movie film events with the temperature–time output from the Dynograph script recorder. Thus, when the strobe fires, the shadowed droplet image is overexposed on one or possibly two frames of movie film and this event is recorded on the script chart recorder.

The technique of droplet injection into the pressurized test chamber was developed using three solenoid valves, one micro-needle valve, and one needle valve. A schematic drawing of the arrangement of the droplet injector solenoid valve assembly is shown in Fig. 10. A pressure difference ($\Delta P = 40$ psi) is applied across the fuel supply tank and the pressure vessel.

EXPERIMENTAL RESULTS

Experimental droplet radius–time and droplet temperature–time histories have been obtained for a n-hexane droplets evaporating in nitrogen and also argon gas environments at a temperature of 548°K and at a range of pressures from

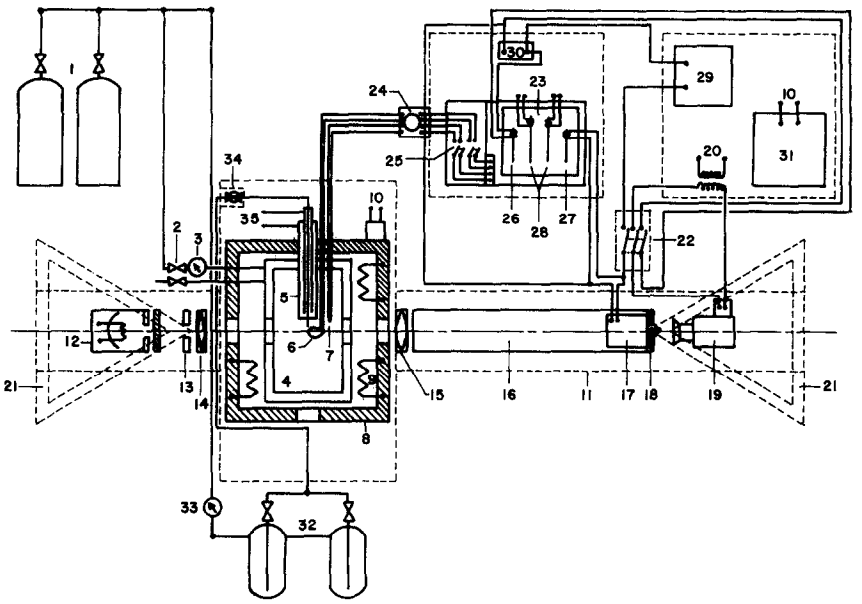

FIG. 9. Schematic diagram of the experimental apparatus.

1. Environment gas supply tanks.
2. Valves for isolating the gas environment and for purging of the environment gas in the pressure vessel.
3. Pressure gauge for measuring the environment gas pressure.
4. Pressure vessel.
5. Injector cooling jacket to prevent the liquid fuel from evaporating before injection.
6. A 0·002 in. wire diameter droplet support thermocouple.
7. A 0·065 in. wire diameter thermocouple for sensing the temperature of the gas environment.
8. Electric furnace.
9. Electrical resistance heaters of furnace.
10. Furnace electrical power connections.
11. Aluminum channel bed supporting the optical bench and camera.
12. Projection bulb light source with ground glass diffusing screen.
13. Iris diaphragm.
14. Condenser lens.
15. A 209·5 mm focal length Bausch and Lomb lens with variable *f* stops.
16. A 10 cm square tube by 110 cm long which prevents stray light from falling on ground glass screen.
17. Electronic strobe unit described in reference [33] modified for long flash duration.
18. Ground glass screen.
19. Bolex 16 mm movie camera with motor drive.
20. Bolex motor control transformer.
21. Tri-pod supports for aluminum channel bed.
22. Remote 3-pole momentary contact switch for triggering of the camera, recorder event markets, strobe unit, and electric clock.
23. Two channel Dynograph Type RS Recorder.
24. Ice (cold junction) bath for thermocouples.
25. Two double pole double throw switches for interrupting the signal from the thermocouples to the recorder.
26. Left event marker of recorder used to indicate the time interval on the recorder output paper that the movie camera was operating
27. Right event marker of recorder used to indicate when the electronic strobe was fired.
28. Left and right channel recorder pens.
29. Synchroneous motor (60 rpm), two lobed cam, and micro-switch assembly for tripping the right event marker and electronic strobe (at a 2/s rate) only when remote switch is closed.
30. A 6V d.c. battery for energizing the two event markers and for providing a 6 V pulse to trigger the electronic strobe.
31. Furnace electrical power controls—variable 240 V a.c.
32. Liquid fuel storage tanks.
33. Pressure gauge for measuring the fuel tank pressure.
34. Droplet injector solenoid valve assembly.
35. Electric clock.
36. Injector coolant input and output.

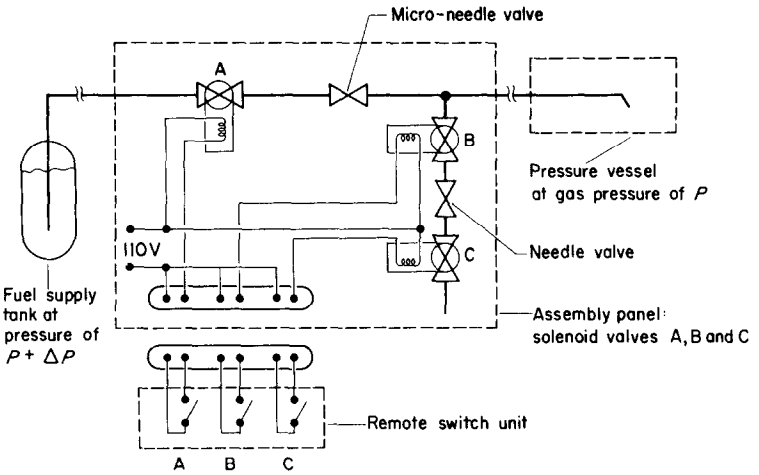

FIG. 10. Schematic diagram illustrating the technique of droplet injection.

6·8 atm to 102 atm. Duplicated experimental runs were made for two particular sets of conditions to check the reproducibility of the results. Three characteristics of each run, the initial temperature of the droplet, the initial size of the droplet, and the time for droplet evaporation were used to check the reproducibility of the experiments. Table 1 summarizes the results giving the mean value and standard deviation of the three characteristics for both sets of experimental conditions.

Table 1. *Reproducibility of experimental results*

Set 1: Five runs of n-hexane-nitrogen at 548°K and 102 atm

	$T_l(\tau = 0)$ (°K)	R_0 (μ)	t_v (s)
Mean	359	400	0·416
Standard deviation	2	22	0·028

Set 2: Six runs of n-hexane-nitrogen at 548°K and 82 atm

	$T_l(\tau = 0)$ (°K)	R_0 (μ)	t_v (s)
Mean	403	350	0·407
Standard deviation	4	12	0·035

A sequence of enlarged 16 mm frames showing the droplet size–time relationship for an n-hexane droplet evaporating in nitrogen gas is presented in Fig. 11. The symbols below each photograph refer to the frame number in the sequence of frames. For example, F-1 refers to frame one of the sequence; F-7 refers to frame seven in the sequence; F-23 refers to the twenty-third frame in the chronological sequence of photographs; and so forth. In some of the sequences of photographs depicting droplet evaporation, an apparent downward motion of vapor was observed in the later frames. A possible explanation of this observation is that the motion is induced by density differences between the gas in the neighbourhood of the droplet and the hotter ambient gas below.

The experimental radius–time histories have been obtained by the following technique. The projected areas of the silhouetted droplet images on the 16 mm movies obtained from experiment were measured using a photographic image scanning device. The device that was used to process the photographic data is the CHLOE system at the Applied Mathematics Division of Argonne National Laboratory, Illinois. Detailed description of the CHLOE system are

given by Butler [34] and Clark and Miller [35]. The CHLOE system consists of a digital computer and an optical cathode ray tube scanner, the latter being under control of the computer. The spot of light from the cathode ray tube is projected onto the film and the light transmitted through the film is viewed by a photomultiplier by means of which a decision is made regarding the density of the film at the circle and by solving for the radius. The frame sequence–time relationship was known through synchronization of the camera and recorder, and an effective radius–time history was then obtained.

Some of the results showing the effects of pressure on the droplet temperature–time and radius–time histories are presented in Fig. 12 for n-hexane droplets evaporating in a nitrogen gas

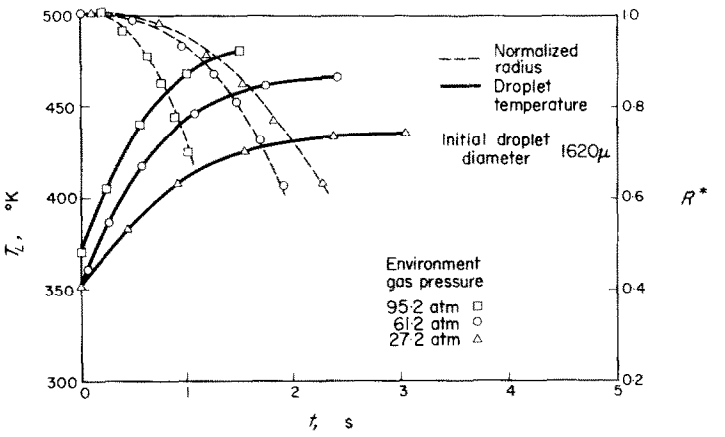

FIG. 12. The effect of pressure on the droplet temperature–time and radius–time histories for n-hexane droplets evaporating in nitrogen gas at an environment temperature of 548°K.

point in question. Although the CHLOE system can recognize up to eight quantized density levels, it was only necessary for the system to distinguish between the light (background) and the dark (silhouetted droplet image) areas of the movie frame. The information from the cathode ray tube scanner was processed with the aid of supporting computer programming and the projected area of the silhouetted droplet image was obtained in arbitrary "CHLOE area" units. Several frames of a silhouetted diamond image of known film magnification and size were scanned along with the experimental film data so that the droplet projected areas could be calculated in physical units. An effective droplet radius was then calculated by equating the measured droplet image area to the area of a

environment and are presented in Fig. 13 for n-hexane droplets evaporating in an argon gas environment. The effect of droplet size on the temperature–time and radius–time histories for n-hexane droplets evaporating in a nitrogen gas environment at 100 psi is shown in Fig. 14.

COMPARISON OF THEORETICAL PREDICTIONS TO EXPERIMENTAL MEASUREMENTS

The procedure for comparing the theoretical predictions for the droplet temperature–time and radius–time histories with the experimental measurements is to choose a theoretical prediction for the droplet temperature–time history that matches with the experimental one. Then, the dimensionless evaporation time and the

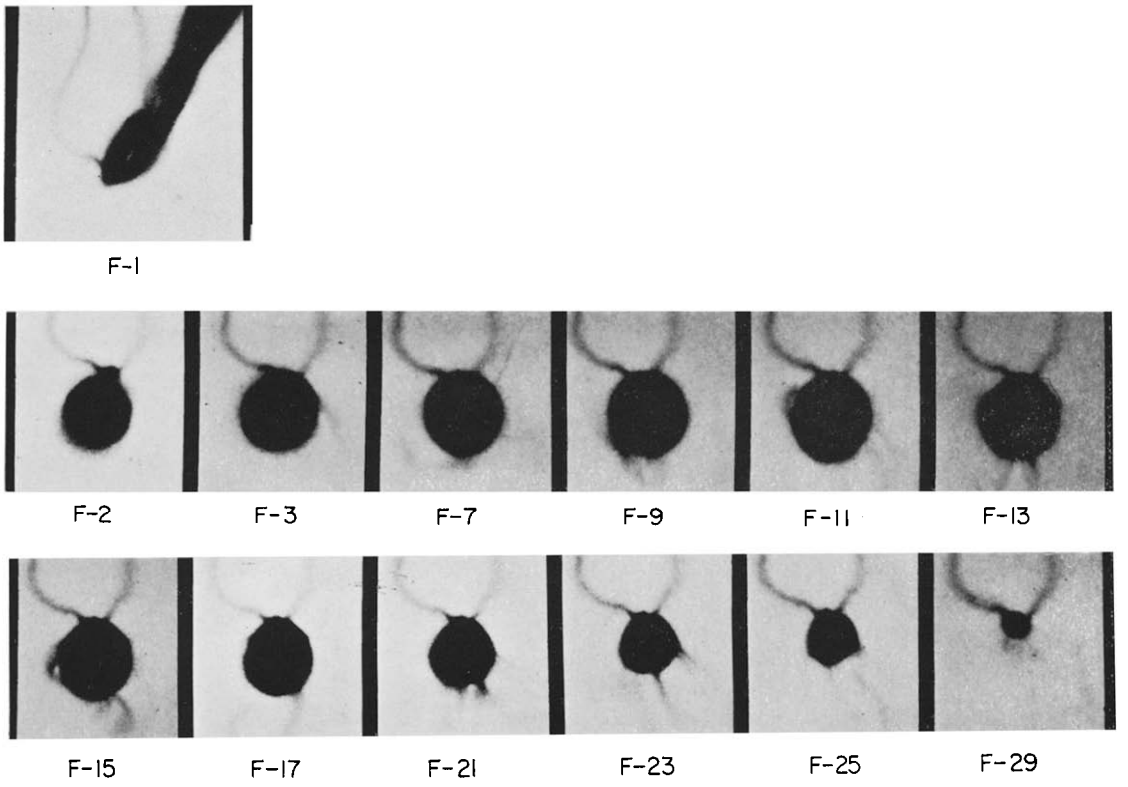

FIG. 11. Sequence of enlarged 16mm frames for experimental run 47-3.2. The event in frame two (F-2) is designated zero time of the run.

[*facing page 846*]

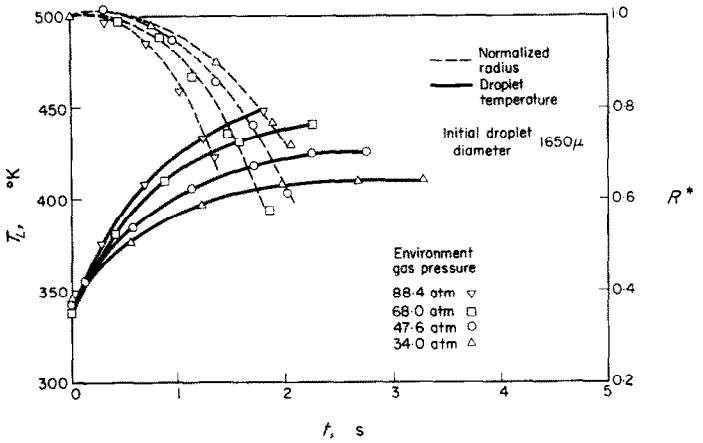

FIG. 13. The effect of pressure on the droplet temperature–time and radius–time histories for n-hexane droplets evaporating in argon gas at an environment temperature of 548°K.

physical evaporation time are assumed equivalent and by substituting the two evaporation times into

$$t^* = \frac{Dt}{R_0^2} \tag{42}$$

with R_0 known from experiment, an effective diffusion coefficient is calculated. The effective diffusion coefficient, D_{eff}, is then compared with the molecular diffusion coefficient calculated from a formula recommended by Reid and Sherwood [36]. To illustrate the method, the comparison of the theoretical prediction to the experimental results for a droplet evaporating at 6·8 atm will be discussed. The theoretical predictions for the droplet temperature–time history at 6·8 atm for three Lewis Numbers are given in Fig. 3. Of the three predictions for the droplet temperature–time history the run with a Lewis Number corresponding to 0·375 is chosen. The

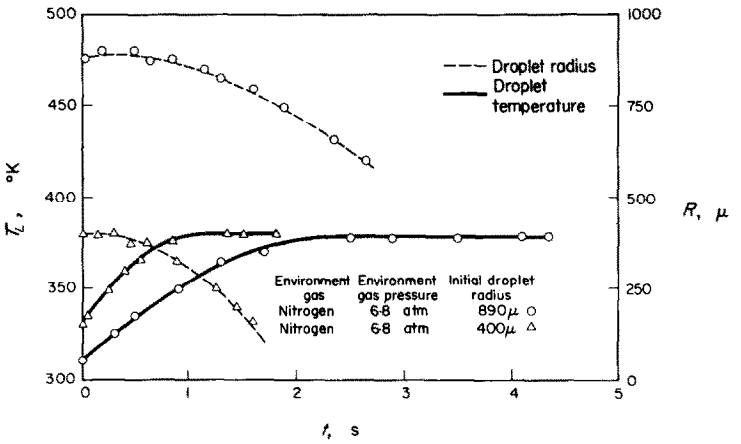

FIG. 14. The effect of droplet size on the temperature–time and radius–time histories.

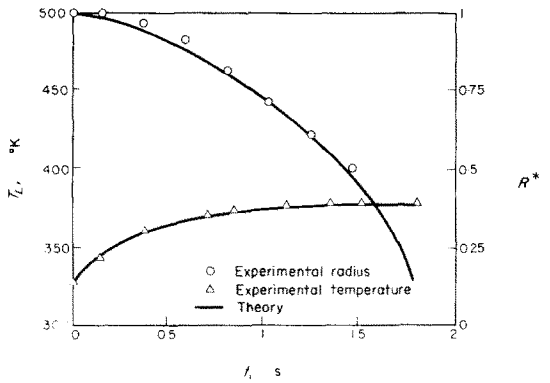

FIG. 15. Comparison of the theoretical predictions to experimental measurements for n-hexane droplet evaporating in nitrogen gas at an environment temperature of 548°K and an environment pressure of 6·8 atm.

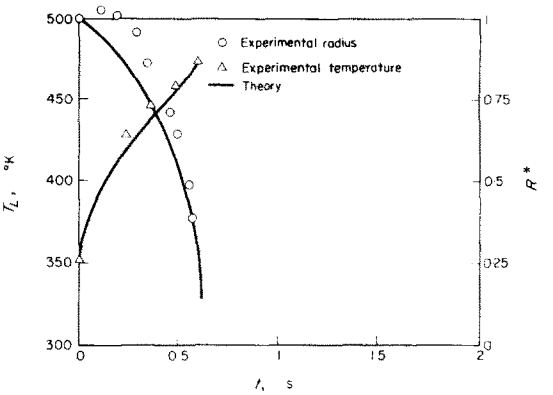

FIG. 17. Comparison of the theoretical predictions to experimental measurements for n-hexane droplet evaporating in nitrogen gas at an environment temperature of 548°K and an environment pressure of 81·6 atm.

asymptotic droplet temperature of this prediction corresponds to the asymptotic droplet temperature found from experiment. The dimensionless and physical times for evaporation are assumed equivalent in their respective time coordinate scales. The initial size of the droplet is given from experiment and with the aid of equation (42) the effective diffusion coefficient is calculated. The molecular diffusion coefficient is calculated using the formula given in Reid and Sherwood [36] given a film temperature, T_{g_f}, defined by $T_{g_f} = (\bar{T}_L + T_\infty)/2$. the environment pressure, and the properties of the binary mixture (n-Hexane–nitrogen). The mean temperature of the liquid droplet, $\bar{T}_L$, is defined in the list of symbols. The results are given in Table 2 and the comparison of the theoretical prediction to experimental measurement for the droplet temperature–time and radius–time histories for an n-hexane–nitrogen system for pressures of 6·8, 20·4, 81·6 and 102 atm are shown in Figs. 15–18.

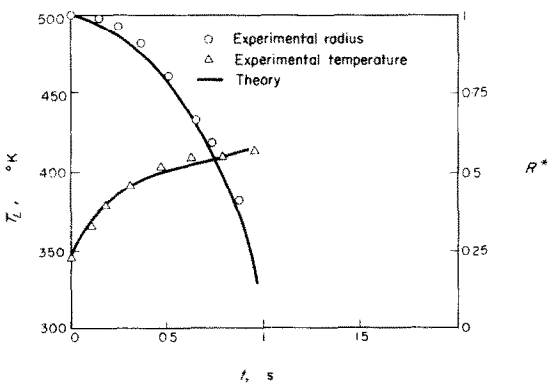

FIG. 16. Comparison of the theoretical predictions to experimental measurements for n-hexane droplet evaporating in nitrogen gas at an environment temperature of 548°K and an environment pressure of 20·4 atm.

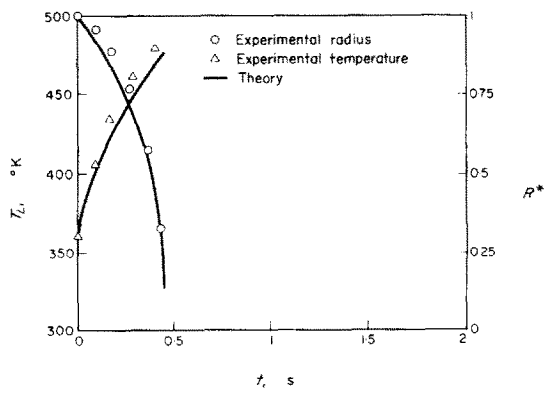

FIG. 18. Comparison of the theoretical predictions to experimental measurements for n-hexane droplet evaporating in nitrogen gas at an environment temperature 548°K and an environment pressure of 102 atm.

Table 2. Comparison of the molecular diffusion coefficient with the effective diffusion coefficient
Fuel: n-Hexane
Environment gas: Nitrogen
Environment temperature: 548°K

P_T (atm)	R_0 (μ)	$T_L(\tau = 0)$ (°K)	t_v (s)	N_{Le}	T_{af} (°K)	D_{eff} (cm²/s)	D_M (cm²/s)	D_{eff}/D_M
6·8	410	329	1·826	0·375	457	0·0292	0·0250	1·17
	420	335	1·952	0·375	458	0·0281	0·0251	1·12
20·4	350	346	0·984	0·425	470	0·0184	0·0088	2·09
40·8	440	366	1·046	0·425	478	0·0146	0·0046	3·21
81·6	400	353	0·618	0·425	486	0·0096	0·0023	4·12
102	430	361	0·458	0·425	486	0·0105	0·0017	6·16

CONCLUSIONS

1. Reproducible temperature–time and radius–time histories for droplets evaporating in a quiescent environment at high ambient temperature and pressure have been obtained and these experimental results aid in the understanding of high temperature and high pressure evaporation phenomena.

2. A droplet evaporation model was formulated that accounts for the transient character of the phenomena, includes the effect of the motion of the droplet boundary on the governing equations, and accounts for the effects of the non-ideal gas behavior in the boundary conditions.

3. The effects of the more realistic non-ideal behavior of the gas phase in calculating the local vapor–liquid equilibrium mole fraction and the energy requirements for phase change which includes the effects of the inert environment are important for the calculation of the temperature–time and radius–time histories of evaporating droplets especially at the higher pressures. The above conclusion means that the more cumbersome technique of calculating the vapor–liquid equilibrium mole fraction and the enthalpy for phase change must be used and if possible these calculations should be supported with experimental data. For the n–hexane–nitrogen system experimental equilibrium mole fraction values were available so a check on the mole fraction calculation was possible. However, the enthalpy for phase change calculation was not supported by experimental data or known reliable tabulated data and the results of this calculation are in doubt. The derivation of this expression involves the derivatives of the equation of state that is used for the mixture and thus serious inaccuracies for the value of the enthalpy for phase change may result.

4. The results of the comparison of the theoretical prediction for the droplet temperature–time and radius–time histories to the experimental measurements, presented in Table 1, indicate that the nature of the mass transport mechanisms may not be molecular since the ratio of the effective diffusion coefficient to the molecular diffusion coefficient as calculated from existing correlations departs greatly from unity at the high chamber pressures. However, investigators who are concerned with droplet evaporation phenomena at high ambient temperatures and pressures for applications to rocket engine design and modeling have, in the past, used molecular diffusion coefficients in their predictions of evaporation rates. The results presented here suggest that a more realistic diffusion coefficient should be used in such analyses.

5. To provide a further check on this droplet evaporation theory, a model should be investigated that would include the variation of the thermal and physical properties in the boundary

layer. However, such an analysis although more complex than the present work (due to the non-linear character of the governing equations) would also be handicapped since a theory for variable mass diffusivity as a function of composition, temperature and pressure would be required.

REFERENCES

1. R. D. INGEBO, Vaporization rates and heat transfer coefficients for pure liquid drops, NACA TN 2368 (1951).
2. R. D. INGEBO, Study of pressure effects on the vaporization rate of drops in gas streams, NACA TN 2850 (1953).
3. W. E. RANZ and W. R. MARSHALL, JR., Evaporation from drops I and II, *Chem. Engng Prog.* **48**, 141, 173 (1952).
4. M. M. EL WAKIL, O. A. UYEHARA and P. S. MYERS, A theoretical investigation of the heating-up period of injected fuel droplets vaporizing in air, NACA TN 3179 (1954).
5. M. M. EL WAKIL, R. J. PRIEM, H. J. BRIKOWSKI, P. S. MYERS and O. A. UYEHARA, Experimental and calculated temperature and mass histories of vaporizing fuel drops, NACA TN 3490 (1956).
6. R. J. PRIEM, G. L. BORMAN, M. M. EL WAKIL, O. A. UYEHARA and P. S. MYERS, Experimental and calculated histories of vaporizing fuel drops, NACA TN 3988 (1957).
7. T. P. TORDA, S. BUSENBERG, J. KAUFFMANN and R. STEINKE, Rational design procedures for liquid propellant rocket motors, Proceedings of the Fifth International Symposium on Space Technology and Science, Tokyo (1963).
8. R. J. PRIEM and M. F. HEIDMANN, Propellant vaporization as a design criterion for rocket engine combustion chambers, NASA TR R-6 (1960).
9. S. LAMBIRIS, L. P. COMBS and R. S. LEVINE, Stable combustion processes in liquid propellant rocket engines, combustion and propulsion. *Fifth AGARD Colloquium: High Temperature Phenomena*. MacMillan, New York (1963).
10. R. J. PRIEM, M. F. HEIDMANN and J. C. HUMPHREY, A study of sprays formed by two impinging jets, NACA TN 3835 (195).
11. D. A. BITTKER, An analytical study of turbulent and molecular mixing in rocket combustion, NACA TN 4321 (1958).
12. BITTKER and R. S. BROKAW, An estimate of chemical space heat rates in gas-phase combustion with applications to rocket propellants, Paper No. 824–59, American Rocket Society (1959).
13. T. P. TORDA, Aerothermochemistry of jet-propulsion liquid-propellant rocket motors, Symposium on Thermodynamics of Jets and Rocket Propulsion, A.I.Ch.E. (1959).
14. T. P. TORDA, Combustion instability of liquid propellant rocket engines—notes on the state of the art and proposed areas of investigations, presented to the AFAOR, Armour Research Foundation TM D-29 (1962).
15. L. P. COMBS, Calculated propellant droplet heating under F-1 combustion chamber conditions. Rocketdyne RR 64-25 (1964).
16. P. R. WIEBER, Calculated temperature histories of vaporizing droplets to the critical point, *AIAA Jl* **1**, 2764.
17. M. HERSCH, A mixing model for rocket engine combustion, NASA TN D-2881 (1965).
18. D. B. SPALDING, Theory of partical combustion at high pressures, *A.R.S. Jl* **29**, 828 (1959).
19. T. A. BRZUSTOWSKI, Chemical and physical limits on vapor-phase diffusion flames of droplets, *Can. J. Chem. Engng* (1965).
20. T. P. TORDA and R. L. MATLOSZ, Liquid droplet evaporation in stagnant high pressure and high temperature environment, NASA CR-72373 (1968).
21. R. L. MATLOSZ, Liquid droplet evaporation in a stagnant high pressure and high temperature environment, M.S. Thesis (1968).
22. T. P. TORDA and R. L. MATLOSZ, Investigation of liquid propellants in high pressure and high temperature gaseous environments, *XIXth International Astronautical Congress, Propulsion Re-entry Physics*, Vol. 3, Pergamon Press, Oxford (1970).
23. F. A. WILLIAMS, On the assumptions underlying droplet vaporization and combustion theories, *J. Chem. Phys.* **33**, 133 (1960).
24. J. L. DUDA and J. S. VRENTAS, Mathematical analysis of bubble dissolution, *A.I.Ch.E. Jl* **15**, 351 (1969).
25. J. A. MANRIQUE and G. L. BORMAN, Calculations of steady state droplet vaporization at high ambient pressures, *Int. J. Heat Mass Transfer* **12**, 1081 (1969).
26. L. N. CANJAR and F. S. MANNING, *Thermodynamic Properties and Reduced Correlations for Gases*. Gulf Publishing, Houston (1967).
27. D. E. STEWART, B. H. SAGE and W. N. LACEY, Volumetric behavior of n-hexane in liquid phases, *Ind. Engng Chem.* **46**, 2529 (1954).
28. P. L. CHUEH and J. M. PRAUSNITZ, Calculation of high-pressure vapor–liquid equilibria, *Ind. Engng Chem.*, **60** (3), 34 (1968).
29. P. L. CHUEH and J. M. PRAUSNITZ, Vapor–liquid equilibria at high pressures. Vapor-phase fugacity coefficients in nonpolar and quantum-gas mixtures, *I/EC Fundamentals* **6**, 492 (1967).
30. J. M. PRAUSNITZ, *A.I.Ch.E. Jl* **5**(3) (1959).
31. R. S. POSTON and J. J. MCKETTA, Vapor–liquid equilibrium in the n-hexane–nitrogen system, *J. Chem. Engng Data* **11**, 364 (1966).
32. W. C. EDMISTER, R. E. THOMPSON and L. YARBOROUGH, Partial enthalpies of components in gas mixtures via Redlich–Kwong equation of state, *A.I.Ch.E. Jl* **9**, 116 (1963).
33. J. CUCCIA, *Popular Electronics* **28**(3), 45 (1968).
34. J. W. BUTLER, *J. Data Management* **3**, 32 (1965).
35. R. CLARK and W. F. MILLER, Computer-based analysis *Methods Comput. Phys.* **5**, 4 (1966).
36. R. C. REID and T. K. SHERWOOD, *The Properties of Gases Liquids: Their Estimation and Correlation*, 2nd ed. McGraw-Hill, New York (1966).

ÉTUDE DE L'ÉVAPORATION D'UNE GOUTTE LIQUIDE DANS UN ENVIRONNEMENT À HAUTE TEMPÉRATURE ET HAUTE PRESSION

Résumé—On a étudié expérimentalement et analytiquement le phénomène d'évaporation d'une goutté dans un milieu stagnant à haute température et haute pression. La vie de la goutte traduite par les lois température-temps et rayon-temps a été étudiée pour des gouttes de n-hexane s'évaporant dans un environnement d'azote ou d'argon. La température du gaz ambiant pour tous les essais expérimentaux d'évaporation de la goutte est de 548°K ; la pression du gaz environnant est de 6,8 ; 20,4 ; 40,8 ; 81,6 et 102 atm. ; le diamètre initial de la goutte est établi dans deux domaines l'un variant de 720 à 910 μ et l'autre de 1420 à 1780 μ.

On a développé pour l'évaporation de la goutte une théorie qui (a) rend compte du caractère transitoire du phénomène (b) comprend l'effet du mouvement de l'interface de la goutte et abandonne ainsi l'approximation quasi-stationnaire qui a été faite dans des théories précédentes (c) tient compte des effets du comportement du gaz non idéal pour le calcul de la condition aux limites d'équilibre vapeur–liquide et aussi des effets de non idéalité de l'enthalpie de vaporisation. On a trouvé que les effets du comportement non idéal de la phase gazeuse sont importants pour les estimations théoriques de la vie de la goutte représentée par les lois température-temps et rayons-temps lors de l'évaporation spécialement aux pressions plus élevées. Les résultats de comparaison de l'estimation théorique pour l'histoire de la goutte représentée par les lois mentionnées ci-dessus avec les mesures expérimentales indiquent qu'à de plus hautes pressions, le transport massique moléculaire ne peut être le mécanisme qui commande le processus d'évaporation. Tandis qu'à une pression de 6,8 atm., le coefficient de diffusion massique effectif est en bon accord avec le coefficient de diffusion massique moléculaire calculé, il lui est 6 fois plus grand à 102 atmosphères.

UNTERSUCHUNG DER TRÖPFCHENVERDAMPFUNG IN EINER UMGEBUNG HOHER TEMPERATUR UND HOHEN DRUCKES

Zusammenfassung—In dieser Arbeit wurden die Phänomene der Tröpfchenverdampfung in einer ruhenden Umgebung bei hoher Temperatur und hohem Druck experimentell und analytisch untersucht. Experimentelle Tröpfchentemperatur/Zeit- und Radius/Zeit-Charakteristika wurden für verdampfende n-Hexantröpfchen in einer Stickstoff- und einer Argonatmosphäre aufgenommen. Die umgebende Gastemperatur für die Verdampfungsmessungen betrug in allen Fällen 548 K; der umgebende Gasdruck betrug 6,8; 20,4; 40,8; 81,6 und 102 atm; der Ausgangsdurchmesser der Tröpfchen wurde in zwei Bereiche eingeteilt, nämlich den von 720–910 μm und den von 1420–1780 μm.

Für die Tröpfchenverdampfung wurde eine Theorie entwickelt, die (a) den zeitlichen Charakter der Phänomene berücksichtigt, (b) den Effekt der Bewegung der Tröpfchengrenze einschliesst und daher die quasistationäre Annäherung früherer Tröpfchentheorien nicht verwendet und (c) den Einflüssen des nichtidealen Verhaltens für die Berechnung der Molenbruchrandbedingung für das Dampf-Flüssigkeitsgleichgewicht und den Effekten der Nichtidentität der Verdampfungsenthalpie Rechnung trägt. Der Einfluss des nichtidealen Verhaltens der Gasphase ist wichtig für die theoretischen Berechnungen der Tröpfchentemperatur/Zeit- und Radius/Zeit-Kurven speziell bei höheren Drücken. Der Vergleich der theoretischen Kurven mit den experimentellen Messungen ergab, dass bei höheren Drücken der molekulare Massentransport nicht der kontrollierende Mechanismus für den Verdampfungsprozess sein kann. Während bei dem niedrigen Druck von 6,8 atm der effektive Massendiffusionskoeffizient gut mit dem berechneten übereinstimmte, war der effektive Massendiffusionskoeffizient bei 102 atm. mehr als sechsmal grösser als der berechnete.

ИССЛЕДОВАНИЕ ИСПАРЕНИЯ КАПЕЛЬ ЖИДКОСТИ В ВЫСОКОТЕМПЕРАТУРНОЙ СРЕДЕ ПРИ ВЫСОКОМ ДАВЛЕНИИ

Аннотация—Проведено экспериментальное и теоретическое исследование явления испарения капель в неподвижной среде при высокой температуре и давлении. Экспериментально определены характер изменения во времени температуры и радиуса капель для н-гексана в атмосфере водорода и аргона. Температура окружающего газа для всех экспериментов по испарению капель была равна 548°К, давление окружающей среды было 6,85 ; 20,4 ; 81,6 и 102 атм. По начальному диаметру капель эксперименты делились на два диапазона—720–910μ и 1420–1470μ.

Разработана теория испарения капель, которая учитывает а. нестационарный характер явления, б. влияние движения границы капель, снимая таким образом ограничения квази-стационарного приближения, принятого в разработанных ранее теориях и в. влияние неидеальности газа на расчет пограничного условия равновесия жидкость-пар (для молей), а также влияние неидеальности газа на расчет пограничного условия равновесия жидкость-пар (для молей), и влияние неидеальности на эпталыпию испарения. Установлено, что влияние неидеального поведения газовой фазы имеет значение для теоретических предсказаний изменения во времени температуры и радиуса испаряющихся капель, особенно при больших давлениях. Результаты сравнения теоретических расчетов изменений во времени температуры и радиуса с экспериментальными данными показали, что при более высоких давлениях молекулярный массоперенос может не быть определяющим механизмом в процессе испарения. При низких давлениях 6,8 атм эффективный коэффициент диффузии массы находился в хорошем соответствии с коэффициентом, рассчитанным по формуле диффузии массы, тогда как при 102 атм эффективный коэффициент диффузии был более, чем в 6 раз выше расчетного значения.